# 3D Lunar Terrain Reconstruction from Apollo Images

Michael J. Broxton[1,2], Ara V. Nefian[2], Zachary Moratto[3], Taemin Kim[1], Michael Lundy[3], and Aleksandr V. Segal[4]

1. NASA Ames Research Center. Moffet Field, CA, 94035
2. Carnegie Mellon University, 3. Stinger-Ghaffarian Technologies Inc.,
4. Stanford University

**Abstract.** Generating accurate three dimensional planetary models is becoming increasingly important as NASA plans manned missions to return to the Moon in the next decade. This paper describes a 3D surface reconstruction system called the *Ames Stereo Pipeline* that is designed to produce such models automatically by processing orbital stereo imagery. We discuss two important core aspects of this system: (1) refinement of satellite station positions and pose estimates through least squares bundle adjustment; and (2) a stochastic plane fitting algorithm that generalizes the Lucas-Kanade method for optimal matching between stereo pair images.. These techniques allow us to automatically produce seamless, highly accurate digital elevation models from multiple stereo image pairs while significantly reducing the influence of image noise. Our technique is demonstrated on a set of 71 high resolution scanned images from the Apollo 15 mission.

## 1 Introduction

Accurate, high resolution Lunar 3D maps will play a central role in NASA's future manned and unmanned missions to the moon. These maps support landing site selection and analysis, lunar landing simulation & training efforts, and computer assisted landing systems. Furthermore, 3D digital elevation models (DEMs) provide valuable information to scientists and geologists studying lunar morphology.

Several recent recent lunar satellite missions, including NASA's Lunar Reconnaissance Orbiter, have returned stereo pairs with unparalleled resolution and image quality. However, historical data collected during the Apollo era still provide some of the best lunar imagery available today [1]. In fact, the Apollo Metric Camera system collected roughly 8,000 images covering roughly 20% of the lunar equatorial zone at a resolution of 10-m/pixel (Figure 1). The extensive coverage and relatively high resolution of this camera makes this data set extremely relevant in modern lunar data processing.

In this paper, we introduce the Ames Stereo Pipeline, a C++ software framework for automated stereogrammetric processing of NASA imagery. We begin

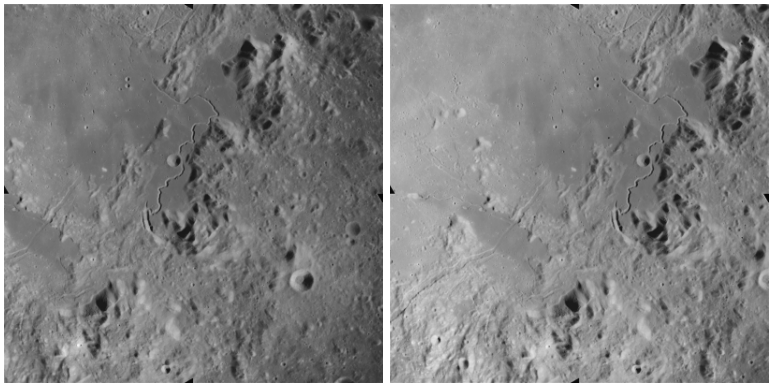

**Fig. 1.** Adjacent Apollo Metric Camera frames (e.g. AS15-M-1135 and AS15-M-1136 shown here) overlap by 80%. This combined with the relatively wide field of view of the camera (74 degrees) results in ideal stereo angles between successive images.

with an overview of this stereo reconstruction framework in Section 2. Then, specific attention is given to two core components of the system: Section 3 describes the bundle adjustment approach for correcting extrinsic camera parameters and co-registering overlapping images; and Section 4 describes our sub-pixel accurate stereo correlation technique. Finally, in Section 5 we present the results of processing Apollo Metric Camera imagery.

## 2 The Ames Stereo Pipeline

The entire stereo correlation process, from raw input images to a point cloud or DEM, can be viewed as a multistage pipeline as depicted in Figure 2.

The process begins with least squares Bundle Adjustment, which is described in Section 3, below. This produces corrected extrinsic camera parameters that are utilized by various camera modeling steps.

Then, the left and right images are aligned using interest points or geometric constraints from the camera models. This step is often essential for performance because it ensures that the disparity search space is bounded to a known area. Next, a prepossessing filter such as the Sign of the Laplacian of the Gaussian filter is used, which has the effect of producing images that are somewhat invariant to differences in lighting conditions [2].

Following these pre-processing steps, we compute the disparity space image $DSI(i, j, d_x, d_y)$ that stores the matching cost between a left image block centered around pixel $(i, j)$ and a right image block centered at position $(i - d_x, j - d_y)$. At this stage, the quality of the match is measured as the normalized cross correlation [3] between two 15x15 pixel image patches. We employ several optimizations to accelerate this computation: (1) a box filter-like accumulator that reduces duplicate operations in the calculation of $DSI$ [4]; (2) a coarse-to-fine pyramid based approach where disparities are estimated using low resolution

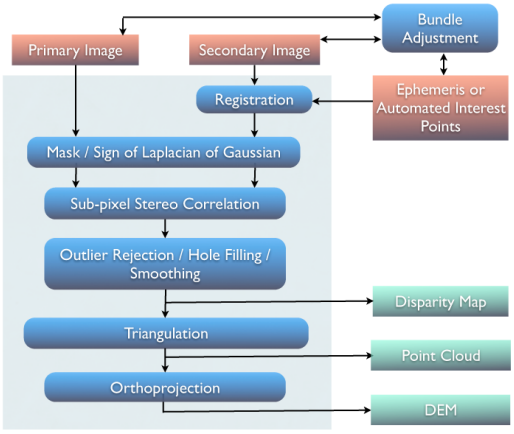


**Fig. 2.** Flow of data through the Ames Stereo Pipeline

images, and then successively refined at higher resolutions; and (3) partitioning of the disparity search space into rectangular sub-regions with similar values of disparity determined in the previous lower resolution level of the pyramid [4].

The *DSI* estimate just described efficiently computes *integer* estimates of disparity between the two images. These estimates are subsequently refined to sub-pixel accuracy using the technique described in Section 4. Finally, in conjunction with the bundle adjusted camera models, the sub-pixel disparity estimates are used to triangulate the location of 3D points as the closest point of intersection of two forward-projected rays emanating from the centers of the two cameras through the matched pixels.

## 3 Bundle Adjustment

The Apollo-era satellite tracking network was highly inaccurate by today's standards with errors estimated to be 2.04-km for satellite station positions and 0.002 degrees for pose estimates in a typical Apollo 15 image [5]. Such errors propagate through the stereo triangulation process, resulting in systematic position errors and distortions in the resulting DEMs (see Figure 3). These errors can be corrected using least-squares bundle adjustment.

In bundle adjustment the position and orientation of the camera are determined jointly with the 3D position of a set of image tie-points points chosen in the overlapping regions between consecutive images. Tie-points are automatically extracted using the SURF robust feature extraction algorithm [6]. Outliers are rejected using the RANSAC method and trimmed to 1000 matches that are spread evenly across the images.

Our bundle adjustment approach follows the method described in [7] and determines the best camera parameters that minimize the projection error given

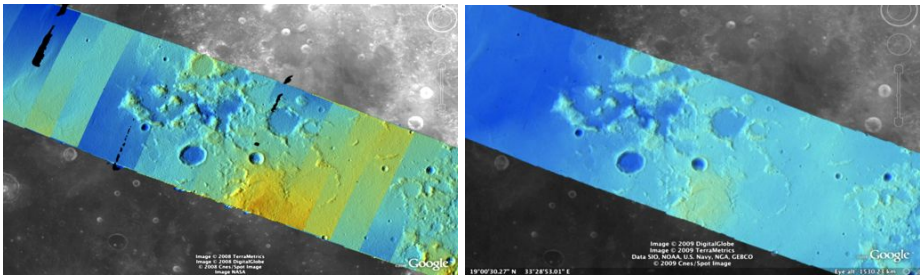

**Fig. 3.** Bundle adjustment is illustrated here using a color-mapped, hill-shaded DEM mosaic from Apollo 15 Orbit 33 imagery. (a) Prior to bundle adjustment, large discontinuities exist between overlapping DEMs. (b) After bundle adjustment, DEM alignment errors are no longer visible.

by $\epsilon = \sum_k \sum_j (I_k - I(C_j, X_k))^2$ where $I_k$ are feature locations on the image plane, $C_j$ are the camera parameters, and $X_k$ are the 3D positions associated with features $I_k$. $I(C_j, X_k)$ is an image formation model (i.e. forward projection) for a given camera and 3D point. The optimization of the cost function uses the Levenberg-Marquartd algorithm. Speed is improved by using sparse methods described in [8].

To eliminate the gauge freedom inherent in this problem, we add two addition error metrics to this cost function to constrain the position and scale of the overall solution. First, $\epsilon = \sum_j (C_j^{initial} - C_j)^2$ constrains camera parameters to stay relatively close to their initial values. Second, a small handful of 3D *ground control points* are chosen by hand and added to the error metric as $\epsilon = \sum_k (X_k^{gcp} - X_k)^2$ to constrain these points to known locations in the lunar coordinate frame. In the cost functions discussed above, errors are weighted by the inverse covariance of the measurement that gave rise to the constraint.

## 4 Sub-pixel Stereo Correlation

Apollo images are affected by two types of noise inherent to the scanning process: (1) the presence of film grain and (2) dust & lint particles. The former gives rise to noise in the DEM values that wash out real features, and the latter causes incorrect matches or hard to detect blemishes in the DEM. Attenuating the effect of these scanning artifacts while simultaneously refining the integer disparity map to sub-pixel accuracy has become a critical goal of our system, and is necessary for processing real-world data sets such as the Apollo Metric Camera data.

A common technique in sub-pixel refinement is to fit a parabola to the correlation cost surface in the 8-connected neighborhood around the integer disparity estimate, and then use the parabola's minimum as the sub-pixel disparity value. This method is easy to implement and fast to compute, but exhibits a problem known as pixel-locking: the sub-pixel disparities tend toward their inte-

ger estimates and can create noticable "stair steps" on surfaces that should be smooth [9], [10]. One way of attenuating the pixel-locking effect is through the use of a symmetric cost function [11] for matching the "left" and "right" image blocks.

To avoid the high computational complexity of these methods another class of approaches based on the Lucas-Kanade algorithm [12] proposes an asymmetric score where the disparity map is computed using the best matching score between the left image block and an optimally affine transformed block from the right image. For example, the sub-pixel refinement developed by Stein et. al. [9] lets $I_R(m,n)$ and $I_L(i,j)$ be two corresponding pixels in the right and left image respectively, where $i = m + d_x$, $j = n + d_y$ and $d_x, d_y$ are the integer disparities. They develop a linear approximation based on the Taylor Series expansion around pixel $(i,j)$ in the left image

$$I_L(i+\delta_x, j+\delta_y) \approx I_L(i,j) + \delta_x \frac{dI_L}{d_x}(i,j) + \delta_y \frac{dI_L}{d_y}(i,j) \tag{1}$$

where $\delta_x$ and $\delta_y$ are the local sub-pixel displacements. Let $e(x,y) = I_R(x,y) - I_L(i+\delta_x, j+\delta_y)$ and $W$ be an image window centered around pixel $(m,n)$. The local displacements are not constant accross $W$ and they vary according to:

$$\begin{aligned} \delta_x(i,j) &= a_1 i + b_1 j + c_1 \\ \delta_y(i,j) &= a_2 i + b_2 j + c_2. \end{aligned} \tag{2}$$

The goal is to find the parameters $a_1, b_1, c_1, a_2, b_2, c_2$ that minimize the cost function

$$\mathbf{E}(m,n) = \sum_{(x,y)\in W} (e(x,y)w(x,y))^2 \tag{3}$$

where $w(x,y)$ are a set of weights used to reject outliers. Note that the local displacements $\delta_x(i,j)$ and $\delta_y(i,j)$ depend on the pixel positions within the window $W$. In fact, the values $a_1, b_1, c_1, a_2, b_2, c_2$ that minimize $\mathbf{E}$ can be seen as the parameters of an affine transformation that best transforms the right image window to match the reference (left) image window.

The shortcoming of this method is directly related to the cost function that it is minimizing, which has a low tolerance to noise. Noise present in the image will easily dominate the result of the squared error function, giving rise to erroneous disparity information. Recently, several statistical approaches (e.g. [13]) have emerged to show how stochastic models can be used to attenuate the effects of noise. Our sub-pixel refinement technique [14] adopts some of these ideas, generalizing the earlier work by Stein et. al. [9] to a Bayesian framework that models both the data and image noise.

In our approach the probability of a pixel in the right image is given by the following Bayesian model:

$$\begin{aligned} P(I_R(m,n)) = &\prod_{(x,y)\in W} \mathcal{N}(I_R(m,n)|I_L(i+\delta_x, j+\delta_y), \frac{\sigma_p}{\sqrt{g_{xy}}})P(z=0) + \\ &+ \mathcal{N}(I_R(m,n)|\mu_n, \sigma_n)P(z=1) \end{aligned} \tag{4}$$

The first mixture component ($z = 0$) is a normal density function with mean $I_L(i + \delta_x, j + \delta_y)$ and variance $\frac{\sigma_p}{\sqrt{g_{xy}}}$:

$$P(I_R(m,n)|z=0) = \mathcal{N}(I_R(m,n)|I_L(i+\delta_x, j+\delta_y), \frac{\sigma_p}{\sqrt{g_{xy}}}) \tag{5}$$

The $\frac{1}{\sqrt{g_{xy}}}$ factor in the variance of this component has the effect of a Gaussian smoothing window over the patch. With this term in place, we are no longer looking for a single variance over the whole patch; instead we are assuming the variance increases with distance away from the center according to the inverted Gaussian, and are attempting to fit a global scale, $\sigma_p$. This provides formal justification for the standard Gaussian windowing kernel.

The second mixture component ($z = 1$) in Equation 5 models the image noise using a normal density function with mean $\mu_n$ and variance $\sigma_n$:

$$P(I_R(m,n)|z=1) = \mathcal{N}(I_R(m,n)|\mu_n, \sigma_n) \tag{6}$$

Let $\mathbf{I}_R(m,n)$ be a vector of all pixels values in a window $W$ centered in pixel $(m,n)$ in the right image. Then,

$$P(\mathbf{I}_R(m,n)) = \prod_{(x,y)\in W} P(I_R(x,y)) \tag{7}$$

The parameters $\lambda = \{a_1, b_1, c_1, a_2, b_2, c_2, \sigma_p, \mu_n, \sigma_n\}$ that maximize the model likelihood in Equation 7 are determined using the Expectation Maximization (EM) algorithm. Maximizing the model likelihood in Equation 7 is equivalent to maximizing the auxiliary function:

$$\begin{aligned}\mathbf{Q}(\theta) &= \sum_k P(k|\mathbf{I}_R, \lambda_t) \log P(\mathbf{I}_R, k, \underline{\delta}|\lambda) \\ &= \sum_k \sum_{x,y} P(k|I_R(x,y), \lambda_t) \log P(I_R(x,y)|k,\lambda) P(k|\lambda)\end{aligned} \tag{8}$$

Note that the M step calculations are similar to the equation used to determine the parameters $a_1, b_1, c_1, a_2, b_2, c_2$ in the method presented in [9], except here the fixed set of weights is replaced by the a posteriori probabilities computed in the E step. In this way, our approach can be seen as a generalization of the Lucas-Kanade method. The complete algorithm is summarized in the following steps:

- **Step 1:** Compute $\frac{dI_L}{d_x}(i,j)$, $\frac{dI_L}{d_y}(i,j)$ and the $I_R(x,y)$ values using bilinear interpolation. Initialize the model parameters $\lambda$.
- **Step 2:** Compute iteratively the model parameters $\lambda$ using the EM algorithm (see [14] for details).
- **Step 3:** Compute $\delta_x(i,j)$ and $\delta_y(i,j)$ using Equation 2.
- **Step 4:** Compute a new point $(x', y') = (x, y) + (\delta_x, \delta_y)$ and the $I_R(x', y')$ values using bilinear interpolation.

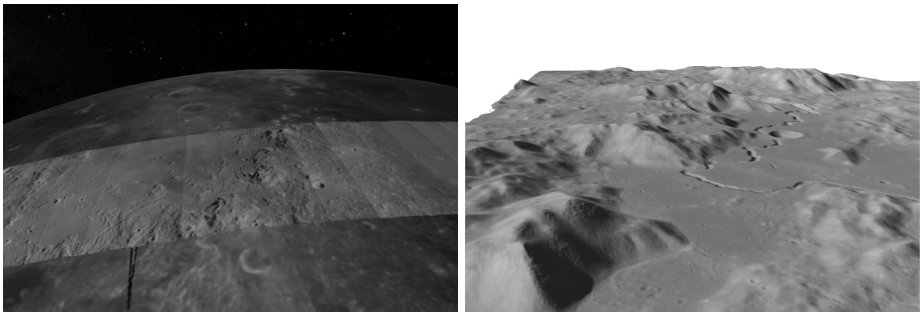

(a) (b)

**Fig. 4.** Hadley Rille and the Apollo 15 landing site derived from Apollo Metric Camera frames AS15-M-1135 and AS15-M-1136. (a) superimposed over the USGS Clementine base map, (b) oblique view.

– **Step 5:** If the norm of $(\delta_x, \delta_y)$ vector falls below a fixed threshold the iterations converged. Otherwise, go to step 1.

Like the computation of the integer $DSI$, we adopt a multi-scale approach for sub-pixel refinement. At each level of the pyramid, the algorithm is initialized with the disparity determined in the previous lower resolution level of the pyramid. This allows the subpixel algorithm to shift the results of the integer $DSI$ by many pixel if a better match can be found using the affine, noise-adapted window.

## 5 Results

The 3D surface reconstruction system described in this paper was tested by processing 71 Apollo Metric Camera images from Apollo 15. Specifically, we chose frames from orbit 33 of the mission, which includes highly overlapping images that span approximately 90 degrees of longitude in the lunar equatorial region. This exercised our algorithms across a wide range of different terrain and lighting conditions. Figure 4 shows the final results in the vicinity of Hadley Rille: the Apollo 15 landing site.

Tests were carried out on a 2.8-GHz, 8-core workstation with 8-GB of RAM. Stereo reconstruction for all 71 stereo pairs took 2.5 days. In the end, the results were merged into a DEM at 40-m/pixel that contained 73,000 x 20,000 pixels.

### 5.1 Bundle Adjustment

Bundle adjustment was carried out as described in Section 3. Initial errors and results after one round of adjustment are shown in columns two and three of Table 1, respectively. Subsequently, any tie-point measurements with image-plane residual errors that were greater than 2 standard deviations from the

mean residual error were thrown out. Bundle adjustment was run a second time yielding slightly improved results shown in column four of the table.

To constrain the scale and absolute position of the solution, 7 ground control points were selected in a triangle wave pattern across the extent of the orbit to tie specific image pixels to known positions in the lunar coordinate frame. The sigma weights for ground control points were based on the resolution of the underlying base map from which ground control points were derived. These were 300-m on the surface and 500-m normal to the surface. Furthermore, the camera station position and pose estimates were constrained to stay close to their initial values based on radio tracking data. Sigma weights for camera parameters were 2-km for position, and 0.01 radians for pose. These values were drawn from historical estimates of Apollo tracking network accuracy as previously discussed.

| Residual Reconstruction | Initial | After Round 1 | After Round 2 |
|---|---|---|---|
| Image Plane | 0.444-mm | 0.012-mm | 0.0075-mm |
| Camera Position | 0-km | 1.31-km | 1.31-km |
| Camera Orientation | 0-mrad | 9.0-rad | 9.1-mrad |
| Ground Control Point | 0-m | 481-m | 465-m |
| Triangulation Error | 911-m | 24.1-m | 15.58-m |

**Table 1.** Residual error at various stages of bundle adjustment. Residual error in the image plane decreases as image tie-point constraints are satisfied. This improvement is made possible as residual "error" for camera position, orientation and ground control points increase to compensate. Triangulation is a measure of the average distance between the closest point of intersection of two forward projected rays for a set of tie-points. Its decrease indicates a substantial improvement in the self-consistency of the DEMs in the data set.

### 5.2 Subpixel Correlation

Film grain and the dust particles are inherent to the scanning process and can significantly limit the accuracy of the stereo processing system. One example where dust particle noise occurs in one of the stereo pair images is shown in detail in Figure 5 (a) and (b). Figure 5 (c) illustrates the integer disparity map obtained by running the fast discrete correlation method described in Section 2. Figure 5 (d), and (e) compares the horizontal sub-pixel disparity maps obtained using the parabola method and the Lucas-Kanade method with the Bayesian approach we introduced in Section 4. The Bayesian approach reduces the "stair-stepping" artifacts apparent in the results from the parabola method. It also demonstrates a degree of immunity to the noise introduced by the speck of dust in (a).

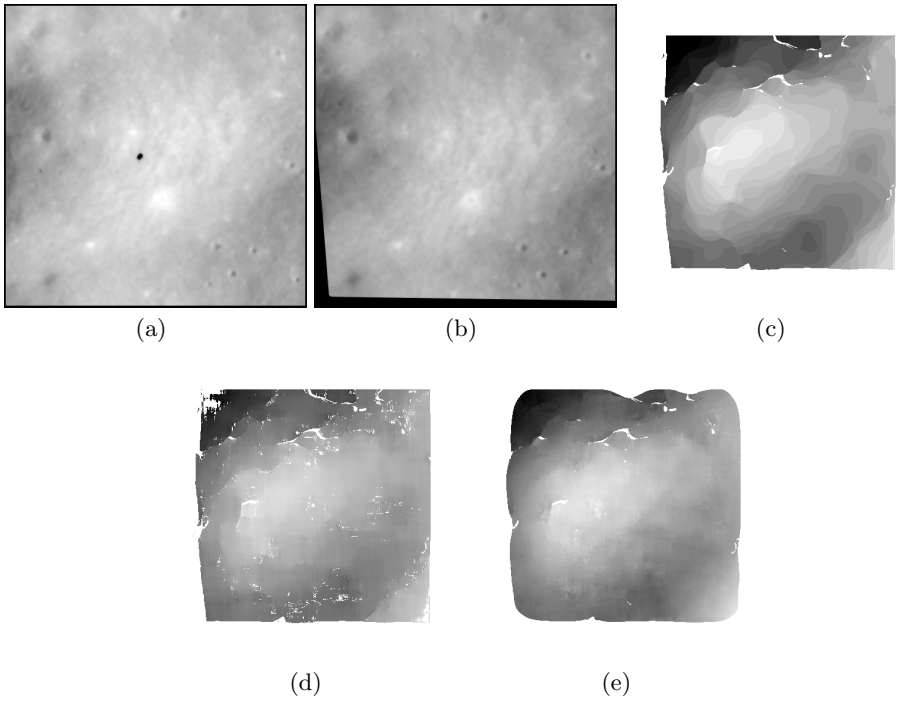


**Fig. 5.** (a) Left Image (with a speck of dust), (b) Right Image, (c) Horizontal integer disparity map, (d) Horizontal disparity map using the parabola method, (e) Horizontal disparity map using the Bayesian approach.

## 6 Conclusions and future work

This paper has introduced a novel statistical formulation for optimally determining stereo correspondence with subpixel accuracy while simultaneously mitigating the effects of image noise. Furthermore, we have successfully demonstrated a significant improvement to the geometric consistency of the results after using least squares bundle adjustment. These techniques were successfully used to process a large, real-world corpus of images and were found to produce useful results. However, this was a preliminary demonstration of these capabilities, and much work remains to quantify residual errors and characterize the degree of noise immunity in our new correlation algorithm. Further research will be directed towards building a comprehensive error model for the 3D surface reconstruction process that can be used to systematically test our system under a variety of different conditions and inputs. Ultimately, we hope to use our technique to process the full collection of over 8,000 Apollo Metric Camera stereo pairs.

## 7 Acknowledgments

We would like to thank Mark Robinson and his team at Arizona State University for supplying high resolution scans of the Apollo Metric Camera images. This work was funded by the NASA Lunar Advanced Science and Exploration Research (LASER) program grant #07-LASER07-0148, NASA Advanced Information Systems Research (AISR) program grant #06-AISRP06-0142, and by the NASA ESMD Lunar Mapping and Modeling Program (LMMP).

## References

1. Lawrence, S.J., Robinson, M.S., Broxton, M., Stopar, J.D., Close, W., Grunsfeld, J., Ingram, R., Jefferson, L., Locke, S., Mitchell, R., Scarsella, T., White, M., Hager, M.A., ad E. Bowman-Cisneros, T.R.W., Danton, J., Garvin, J.: The Apollo Digital Image Archive: New Research and Data Products. In: Proc of the NLSI Lunar Science Conference. (2008) 2066
2. Nishihara, H.: PRISM: A Practical real-time imaging stereo matcher. Optical Engineering **23** (1984) 536–545
3. Menard, C.: Robust Stereo and Adaptive Matching in Correlation Scale-Space. PhD thesis, Institute of Automation, Vienna Institute of Technology (PRIP-TR-45) (1997)
4. Sun, C.: Rectangular Subregioning and 3-D Maximum-Surface Techniques for Fast Stereo Matching. International Journal of Computer Vision **47** (2002)
5. Cameron, W.S., Niksch, M.A.: NSSDC 72-07: Apollo 15 Data User's Guide (1972)
6. Bay, H., Ess, A., Tuytelaars, T., Gool, L.V.: SURF: Speeded Up Robust Features. Computer Vision and Image Understanding (CVIU) **110** (2008) 346–359
7. Triggs, B., Mclauchlan, P., Hartley, R., Fitzgibbon, A.: Bundle adjustment – a modern synthesis (2000)
8. Hartley, R.I., Zisserman, A.: Multiple View Geometry in Computer Vision. Second edn. Cambridge University Press, ISBN: 0521540518 (2004)
9. Stein, A., Huertas, A., Matthies, L.: Attenuating stereo pixel-locking via affine window adaptation. In: IEEE International Conference on Robotics and Automation. (2006) 914 – 921
10. Szeliski, R., Scharstein, D.: Sampling the Disparity Space Image. IEEE Transactions on Pattern Analysis and Machine Intelligence (PAMI) **26** (2003) 419 – 425
11. Nehab, D., Rusinkiewicz, S., Davis, J.: Improved sub-pixel stereo correspondences through symmetric refinement. Computer Vision, IEEE International Conference on **1** (2005) 557–563
12. Baker, S., Gross, R., Matthews, I.: Lucas-Kanade 20 Years On: A Unifying Framework. International Journal of Computer Vision **56** (2004) 221–255
13. Cheng, L., Caelli, T.: Bayesian stereo matching. Computer Vision and Pattern Recognition Workshop, 2004. CVPRW '04. Conference on (2004) 192–192
14. Nefian, A., Husmann, K., Broxton, M., To, V., Lundy, M., Hancher, M.: A Bayesian formulation for sub-pixel refinement in stereo orbital imagery . International Conference on Image Processing (2009)